Author Manuscript

Author Manuscript

Author Manuscript

Author Manuscript

HHS Public Access

Author manuscript

IEEE Trans Med Imaging. Author manuscript; available in PMC 2019 May 01.

Published in final edited form as:

IEEE Trans Med Imaging. 2018 May ; 37(5): 1214–1223. doi:10.1109/TMI.2017.2780855.

Probe Oscillation Shear Wave Elastography: Initial *In Vivo* Results in Liver

Daniel C. Mellema [Student Member, IEEE],
Mayo Clinic Graduate School of Biomedical Sciences and the Department of Radiology, Mayo Clinic, Rochester, MN 55905 USA

Pengfei Song [Member, IEEE],
Department of Radiology, Mayo Clinic, Rochester, MN 55905 USA

Randall R. Kinnick [Senior Member, IEEE],
Department of Physiology and Biomedical Engineering, Mayo Clinic, Rochester, MN 55905 USA

Joshua D. Trzasko [Senior Member, IEEE],
Department of Radiology, Mayo Clinic, Rochester, MN 55905 USA

Matthew W. Urban [Senior Member, IEEE],
Department of Radiology, Mayo Clinic, Rochester, MN 55905 USA

James F. Greenleaf [Life Fellow, IEEE],
Department of Physiology and Biomedical Engineering, Mayo Clinic, Rochester, MN 55905 USA

Armando Manduca [Member, IEEE], and
Department of Physiology and Biomedical Engineering, Mayo Clinic, Rochester, MN 55905 USA

Shigao Chen [Member, IEEE]
Department of Radiology, Mayo Clinic, Rochester, MN 55905 USA

Abstract

Shear wave elastography methods are able to accurately measure tissue stiffness, allowing these techniques to monitor the progression of hepatic fibrosis. While many methods rely on acoustic radiation force (ARF) to generate shear waves for two-dimensional (2D) imaging, probe oscillation shear wave elastography (PROSE) provides an alternative approach by generating shear waves through continuous vibration of the ultrasound probe while simultaneously detecting the resulting motion. The generated shear wave field in *in vivo* liver is complicated, and the amplitude and quality of these shear waves can be influenced by the placement of the vibrating probe. To address these challenges, a real-time shear wave visualization tool was implemented to provide instantaneous visual feedback to optimize probe placement. Even with the real-time display, it was not possible to fully suppress residual motion with established filtering methods. To solve this problem, the shear wave signal in each frame was decoupled from motion from other sources through use of a parameter-free empirical mode decomposition (EMD) before calculating shear wave speeds. This method was evaluated in a phantom as well as in *in vivo* livers from five volunteers. PROSE results in the phantom as well as *in vivo* liver correlated well with independent measurements using the commercial General Electric Logiq E9 scanner.

Author Manuscript Author Manuscript Author Manuscript Author Manuscript

Index Terms

high frame-rate; liver elastography; mechanical vibration; real-time imaging; ultrasound elastography

I. Introduction

Many elastography techniques have been developed, which are capable of obtaining measurements in the liver [1–8]. These methods utilize the shear wave propagation speed to quantitatively estimate the stiffness of soft tissue. Magnetic resonance elastography (MRE) was one of the first methods used for non-invasive measurements of hepatic stiffness [5]. In liver MRE, shear waves are delivered through a pneumatic driver placed on the abdomen, inducing wave propagation throughout the entire liver. Current MRE acquisitions are capable of measuring shear wave motion in three orthogonal directions for two-dimensional (2D) slices as well as three-dimensional (3D) volumes. The ability to image motion in all directions has the added benefit of allowing the use of the curl to decouple longitudinal waves from shear waves [9]. MRE relies on continuous wave (CW) shear wave fields, therefore stiffness can be related to wavelength and estimated with local frequency estimation (LFE) [10] or from the fundamental wave equation used in direct inversion (DI) [11]. With good shear wave coverage as well as the capabilities of detecting motion in three orthogonal directions, MRE is capable of making accurate shear wave speed estimates for large field-of-view. While effective, MRE is expensive and has limited availability.

Ultrasound elastography methods are an inexpensive alternative to MRE. One of the first ultrasound methods capable of making hepatic stiffness measurements was Transient Elastography (TE) [2]. This method uses a small single-element transducer to deliver a mechanical impulse to generate a transient longitudinally polarized shear wave, where the particle motion is in the same direction as the wave propagation. The theoretical explanation of this longitudinally polarized shear wave can be found in [12, 13]. Propagation of the shear wave is detected by the same single-element transducer along its beam axis, and the resulting one-dimensional (1D) motion profile can be utilized to determine a global shear wave speed value through the use of a time-to-peak method [14].

More recently, ultrasound-based methods have utilized acoustic radiation force (ARF) to generate propagating shear waves with cylindrical or conic wave fronts conducive for 2D imaging [1, 3, 7]. ARF-based elastography may use the time-to-peak or time-of-flight method for shear wave speed estimations [1, 3, 4, 7, 15–17]. While very versatile, this technique is limited by ultrasound attenuation and shear wave attenuation. For example, the ultrasound push beam used to generate the shear wave has difficulty penetrating beyond 7-8 cm. Even at shallower depths, the resulting shear wave rapidly attenuates, preventing the method from imaging a large 2D area. Another constraint is that scanners must be equipped with specialized hardware and power supplies to generate the high intensity, long duration push pulses, and imaging frame-rates are typically limited to about 1 Hz to prevent tissue and probe thermal damage [18].

Author Manuscript Author Manuscript Author Manuscript Author Manuscript

Probe Oscillation Shear Wave Elastography (PROSE) has been developed to leverage the increased penetration and coverage of mechanically generated shear waves with the ability to continuously track the motion in 2D [19]. This method generates longitudinally polarized shear waves in the tissue with a monochromatic mechanical vibration of the ultrasound probe. Standard pulse-echo ultrasound detection is used to simultaneously track the resulting shear waves while the probe is in motion. Because ultrasound utilizes changes in individual scatterer's position (relative to the ultrasound transducer) to track motion, the movement of the vibrating transducer between subsequent detections leads to a depth dependent probe motion artifact. The artifact arises as a material compresses when the probe moves through the vibration cycle, with scatterers near the probe moving less (relative to the probe surface) than scatterers further from the probe. This results in a non-linear strain-like artifact, causing a bias in shear wave speed estimates [19].

We have previously shown that the probe motion artifact can be suppressed by symmetric sampling [19]. Symmetric sampling strategically selects the timing of detections when the probe returns to the same location, minimizing any difference in the scatterer's position due to material compression, and retaining the motion from the shear waves (Fig. 1a-c). This method limits detections to single frames twice per vibration cycle, preventing shear wave speeds from being estimated with time-to-peak or phase gradient methods [14, 16, 20]. However, the motion was generated with a single tone vibration source, allowing the use of LFE on a single frame to estimate the shear wave speeds. In practice, it was shown that PROSE was capable of creating shear wave fields with excellent coverage as well as estimating shear wave speeds with a theoretical frame-rate an order of magnitude higher than ARF-based methods [19].

While applying PROSE to *in vivo* cases, it was observed that the symmetric sampling method was unable to suppress all of the residual motion that may be caused by out-of-plane waves and anatomical motion of the subject (Fig. 1d). The addition of residual motion violates the underlying assumption that for at any spatial location there exists a single spatial frequency that is related to the mechanical properties if the vibration source is monochromatic. This results in biased shear wave speed estimates. The use of a simple bandpass filter was attempted to separate the residual motion (long wavelengths) from the shear wave signal (relatively shorter wavelengths), but it was found that the two signals could not be robustly decoupled and Fig. 2a-c illustrates that the reconstructed shear wave speeds were dependent on the cutoff values of the bandpass filter.

To produce accurate shear wave speed estimates that are invariant to the filtering process, it was necessary to utilize other means to remove the residual motion. This work proposes utilizing the Empirical Mode Decomposition (EMD) [21] as a parameter-free approach to separate a signal into a set of components corresponding to distinct instantaneous spatial frequencies, allowing the shear wave signal to be decoupled from artifacts and other motion. This new approach allows PROSE to overcome the previous limitation of acquiring motion from only two symmetric frames per cycle and now provides stable shear wave speed estimates in large field-of-view frames at the regular imaging frame rate of the ultrasound scanner.

Author Manuscript Author Manuscript Author Manuscript Author Manuscript

II. Methods

A. Vibration System

PROSE relies on utilizing a transducer to simultaneously generate and detect longitudinally polarized shear waves. To accomplish this, an in-house voice-coil driven vibration system was co-axially attached to a C5-2v ultrasound curved array (Verasonics Inc., Kirkland, WA) [19]. A 30 Hz monochromatic signal was generated with a function generator (Agilent 33250A, Agilent Technologies, Inc., Santa Clara, CA) and amplified (Crown D150A, Crown Audio, Inc., Elkhart, IN; voltage gain: 26 dB) to drive the voice-coil (BEI Kimco, Vista, CA). Shear waves were generated by placing the vibration system in contact with the object to be imaged.

B. Real-Time Visualization

The resulting motion can be measured using standard pulse-echo ultrasound. A real-time shear wave imaging sequence was utilized to provide visual feedback on shear wave quality, allowing the sonographer to determine the best window for data collection. This was accomplished by acquiring a pair of pulse-echo detections separated by 1 ms. The first detection was a standard B-mode sector image acquired with a diverging wave transmission with four steering angles for coherent compounding (−3°, −1°, +1°, +3°) [22]. Fig. 3 has outlined the field-of-view of this detection in yellow. The second detection still utilized diverging wave transmission with four angle coherent compounding with the same steering angles, but limited the corresponding beamformed region to a smaller square region to reduce computational time (8 cm by 8 cm; Fig. 3 red box). The use of the smaller square area (instead of the full sector) for the second pulse echo event saved time in beamforming, which is important for real-time display. Axial motion of the propagating shear wave was then estimated for the square region using Kasai’s method on the two detection frames [23].

To better visualize the shear waves, a bandpass filter with cutoffs corresponding to shear wave speeds of 0.5 - 6.0 m/s was applied to the square area to suppress the probe motion artifact, which has long wavelengths and thus high shear wave speeds. Motion data in the square area was mirrored in both dimensions before applying the Fourier transform (for bandpass filtering) to avoid boundary discontinuity artifacts. After single frame processing, the shear wave motion was superimposed on the B-mode and displayed in real-time on screen (Fig. 3). This approach interleaved B-mode and shear wave imaging to save computation time while providing real-time updates of a large sector B-mode image with an 8 cm by 8 cm window display of shear waves. Implementation of this methods resulted in a display frame-rate of about 10 Hz using MATLAB (Mathworks, Natick, MA) running on the Verasonics ultrasound scanner.

The method was not able to directly image wave propagation as the selected vibration frequency was higher than the display frame-rate. However, it was possible to leverage the periodic nature of the shear waves to track wave propagation. Given that the probe’s motion is periodic, the motion detected at a given phase will be identical to the motion detected when the phase differs by an integer number of periods. This allows shear wave motion frames separated by a phase of φ to be visualized with detections spaced as $2\pi n + \varphi$, where n

Author Manuscript Author Manuscript Author Manuscript Author Manuscript

is a positive integer. For this study, n was set such that there was about a 100 ms delay between detections to allow sufficient time for beamforming, processing, and display of the previous shear wave frame. A schematic describing the acquisition timing is shown in Fig. 3.

When an acoustic window with consistent shear wave propagation in the deepest regions was identified with the real-time shear wave visualization, the detection was switched to an acquisition sequence that tracked motion across the full sector, collecting 100 frames with four angle compounding (−3°, −1°, 1°, and 3° steering angles) at an effective frame-rate of 1 kHz. All of the data were saved and processed offline.

C. Empirical Mode Decomposition

EMD is a method developed to iteratively separate non-stationary signals into multiple basis functions according to the inherent structure of the signal [21]. The method serves as a parameter-free approach to decompose complicated signals into intrinsic modes and has been successfully utilized in a number of scientific applications [24–27]. EMD functions by separating a signal into multiple intrinsic mode functions (IMF) which A) have at most one more zero crossing than local maxima; and B) are centered around zero such that the midpoint of the signal's envelope is equal to zero across the entire signal. These IMFs can be extracted from the parent signal through a parameter-free, iterative process of envelope fitting.

To illustrate this process, Fig. 4a shows a 1D numerical signal comprised of two shear waves with amplitudes of 0.5 and 1, with wavelengths of 20 and 35 mm, respectively, and a simulated compression with a maximum amplitude of 5 (black line). The EMD process begins by computing the upper and lower envelopes of the signal. The upper envelope can be estimated by identifying all of the positive local maxima (Fig. 4a, black dots) and fitting a spline through the resulting points (Fig. 4a, dashed line). A similar process can be repeated to identify the lower envelope. Next, the midline of the signal is obtained by calculating the mean of the two envelopes at each location, this is represented as the red line in Fig. 4a. The midline is subtracted from the signal to effectively remove any low frequency modulations (Fig. 4b, black).

Once the modulations are removed, the number of zero crossings and local maxima are identified again. If the number of local maxima exceeds the number of zero crossings by more than one, or if the midpoint of the envelope is not identically zero for all points, the resultant signal is not an IMF, and a sifting process is initiated. This sifting process repeats the envelope detection and midline estimation/removal until both criteria are satisfied. For this example, the midline of Fig. 4b (red), has spatial variations requiring the iterative sifting process to be performed to obtain the IMF (Fig. 4c, black). Once an IMF is identified, it is subtracted from the original signal and the process is repeated until the input signal is monotonic and unable to be further decomposed. Fig. 4d shows the second IMF representing the second shear wave signal, with all additional IMFs corresponding to the compression. In practice, it is not feasible to obtain envelopes that result in identically zero midpoints, and instead this criterion is relaxed such that the total deviations of the midpoints are smaller than a predefined threshold.

Author Manuscript Author Manuscript Author Manuscript Author Manuscript

For this work, two established modifications to the EMD were used. First the EMD was extended from 1D to 2D to account for spatial information contained within the wavefield. The 2D case has many similarities to the 1D case, where the envelopes are estimated from fitting the local maxima/minima with a thin-plate spline [28] (2D analog of a 1D spline). Fig. 5a depicts a simulated 2D shear wave signal with probe motion artifact (colored surface) where the envelope is depicted as the black mesh obtained by fitting a thin-plate spline through the local maxima.

In the second modification, the complex extension of EMD [29] was used to process the temporal harmonic of the signal, which was obtained by applying the fast Fourier transform to the temporal dimension and extracting the motion oscillating at the vibration frequency. While the standard EMD seeks to decompose the signal into a series of oscillating intrinsic modes, the complex extension simultaneously utilizes both the real part and imaginary part to decompose the signal into a series of rotating components. This is done by projecting the data at multiple phase angles, and using extrema along those projections to construct the envelope as a complex surface (see Fig. 5b). A more detailed description of this method can be found in the papers by Rilling, *et al*. [29] and Looney *et al*. [30]. The application of EMD to the *in vivo* data used in Fig. 2 allowed the removal of residual motion artifacts and generated stable shear wave speeds maps that were minimally influenced by filter cutoffs (Fig. 6).

D. Phantom Measurement

A CIRS liver fibrosis phantom (Model 039, CIRS Inc.) was imaged with a Verasonics Vantage ultrasound imaging system. A C5-2v ultrasound probe attached to the voice-coil vibration system was used for imaging. The vibration system was manually held on the surface of the phantom with minimal pressure to prevent compression of the phantom. The system was driven with a continuous 100 Hz signal such that the maximum displacement was less than 0.1 mm. The real-time display was used to optimize probe placement, and the second imaging sequence was utilized to collect 100 frames of motion. The field-of-view (FOV) of each frame was 13.8 cm by 21.7 cm. Motion was calculated from the in-phase/quadrature (IQ) data using a 1D autocorrelation method [23].

A temporal and directional filter was applied to the data to reduce the strong reflections caused by shear wave interactions with the hard walls of the phantom and remove any motion not moving at the vibration frequency [31–33]. A temporal Fourier transform was applied to the resulting signal, and the signal corresponding to the vibration frequency (harmonic) was selected for additional processing. A lowpass filter in the spatial frequency domain was applied to the signal to remove high spatial frequency fluctuations (short wavelengths) that can cause errors in EMD envelope detection. For a constant temporal vibration frequency, the shear wave speed is inversely proportional to the spatial frequency. Thus, a spatial frequency filter was used to suppress shear wave speeds below 0.5 m/s (spatial wavelengths below 5 mm at 100 Hz). Because the shear wave speed in the phantom (as well as in liver) will be above 0.5 m/s, this cutoff will reduce noise without removing relevant shear wave information.

Author Manuscript Author Manuscript Author Manuscript Author Manuscript

The EMD was performed on the filtered complex signal. Since there was a limited amount of spatial frequency content in each frame, it was empirically determined from the phantom and *in vivo* data that 3 IMFs were sufficient to separate the shear waves. The IMFs not containing propagating shear waves represented the compression artifact. An estimation of the probe motion artifact was obtained by summing all of the non-propagating IMFs. A spatial frequency filter was applied to the probe motion to remove any wavelengths corresponding to shear wave speeds less than 6.0 m/s. The filtered estimation of the probe motion artifact was subtracted from the temporally filtered - but not spatially filtered - signal to obtain an estimation of the underlying shear wave signal.

After the residual motion was removed from the shear wave signal, as a precaution a second spatial bandpass filter was applied to further reduce spatial noise that may remain from the temporally filtered signal. The cutoffs for the bandpass filter were set to exclude shear waves propagating at less than 0.5 m/s and more than 6.0 m/s, which should still preserve the full biological range of shear wave speed in liver from normal to cirrhosis [34]. A directional filter was applied to remove waves propagating *towards* the transducer as waves from PROSE should primarily propagate *away* from the transducer. Using the B-mode image, a mask was manually drawn corresponding to the phantom boundaries. The mask was applied to the shear wave signal to limit data analysis to be within the phantom. The LFE was applied to the resulting wave field to obtain a shear wave speed image, with the reported mean and standard deviation of shear wave speed estimates calculated from the area within the mask. For comparison, five ARF-based measurements were acquired using a General Electric Logiq E9 (GE Healthcare, Wauwatosa, WI).

E. In Vivo Measurements

Five volunteers were imaged under an IRB approved protocol. Imaging was performed with a Verasonics Vantage ultrasound imaging system. Volunteers were in a supine position with their right side slightly elevated, allowing access to the intercostal spaces. The vibration system was driven with a 30 Hz signal. The vibration amplitude was adjusted under the guidance of real-time shear wave display so that shear waves were clearly visible. The maximal displacement of the probe for the *in vivo* study was less than 1 mm, which was estimated from the compression artifact at the deepest region of the field of view. We used 30 Hz for *in vivo* measurements because shear waves penetrated deeper into the liver at lower frequencies. The imaging sequence described for the phantom was used for detection. The real-time shear wave imaging sequence provided visual feedback on shear wave quality, allowing the sonographer to determine the best intercostal window and probe placement prior to data collection.

The probe was placed in the intercostal space and B-mode imaging was used to select a good acoustic window. Next the probe vibration was activated and the probe orientation was adjusted until there were visually observable shear waves that propagated to the deep regions of the liver. In some cases, the selected window did not have strong shear wave propagation present and the probe was shifted along the intercostal space until visible waves were observed in the deepest regions. The adjustments required to obtain the shear wave field generally took less than 45 seconds. The volunteer was asked to perform a breath hold at

Author Manuscript Author Manuscript Author Manuscript Author Manuscript

end-expiration and shear waves were acquired intercostally within the right liver lobe using the second imaging sequence. The *in vivo* data did not have strong reflections that were observed in the phantom, allowing the initial directional filtering step to be omitted. The application of the EMD and subsequent filtering was identical to that of the phantom study. Similar to the phantom experiment, masks were manually drawn to limit the LFE to operate on motion contained within the liver. While the LFE was performed on all motion within the liver, the reported shear wave speeds were limited to manually selected region-of-interest (ROI) with clear propagating shear waves. For comparison five ARF-based measurements were acquired using the Logiq E9.

To test the reproducibility of PROSE, five repeated PROSE acquisitions were obtained from a healthy volunteer. The acquisition procedure was identical to the previous *in vivo* study, however the probe was removed and placed back onto the volunteer between each acquisitions. Processing was kept consistent with the previous study.

III. Results

Fig. 7 shows the IMF decomposition and corresponding shear wave speed image obtained with PROSE for the homogenous CIRS liver fibrosis phantom. Shear wave propagation is captured within the first three IMFs. The spatial variation in the residual motion (Fig. 7e) was due to standing waves within the phantom and did not contribute to propagating shear wave signal. The mean and standard deviation of the shear was speed measured with PROSE was 2.49 ± 0.25 m/s compared to a value of 2.46 ± 0.06 m/s reported by the Logiq E9.

The B-mode image, the shear wave field after artifact removal, and the LFE reconstructions from two of the five volunteers are shown in Fig. 8. Fig. 9 shows the detected motion and the IMF decomposition for one of the volunteers. The mean and standard deviation of shear wave speeds within the manually selected ROI from a single PROSE acquisition from each of the five volunteers are shown in Table 1 (average ROI size was 52.3 cm^2). As the ROI obtained from the Logiq E9 were much smaller (approximately 2.0 cm^2), the means and standard deviations were calculated from the five mean shear wave speeds from the five acquisitions. Note that the standard deviations in Table 1 are thus not comparable across columns. There was good agreement between the mean shear wave speeds reported by PROSE and those reported by the Logiq E9. A comparison of the estimated shear wave speeds is shown in Fig. 10. A linear fit and Pearson's correlation was performed on the shear wave speed measurements, resulting in a slope of 1.068 and a correlation value of 0.955 (95% confidence 0.463 to 0.997) with a p-value of 0.013. As the liver is viscoelastic, it is expected that the Logiq E9 will report higher shear wave speeds than PROSE (due to shear wave speed dispersion effects) because the Logiq E9 should have a higher shear wave frequency than PROSE. However, we did not observe a substantial difference in this preliminary study. This may be due to the small sample size of this study. Future studies with larger sample sizes will be needed to characterize the magnitude of this effect.

Fig. 11 shows the mean and standard deviation of the shear wave speeds for each of the five repeated scans on a single volunteer (Table 1, Volunteer 5). The mean and standard deviation

Author Manuscript Author Manuscript Author Manuscript Author Manuscript

of the mean shear wave speeds reported for all five trials was 1.33 ± 0.06 m/s, which is comparable to the Logiq E9 results in Table 1.

IV. Discussion

This work proposed two solutions to address challenges that arose when using PROSE for *in vivo* imaging: the identification of suitable imaging windows and decoupling the shear waves from other artifacts. The real-time display provided visual feedback, allowing the sonographer to quickly survey multiple imaging windows. This provided an imaging window with visible shear wave propagation at depths of 12 cm. Even with the real-time display, it was not possible to fully suppress effects from probe motion, reflections, or other confounding factors. This prevented decoupling of the shear wave signal from artifacts and resulted in instability in the shear wave speed estimates. EMD was able to successfully decouple the shear waves and allowed accurate and stable shear wave speed estimates over a large field-of-view. This is illustrated in Fig. 2 and Fig. 6 as shear wave speed estimates from symmetrically sampled frame increased by 0.66 m/s as the bandpass filter cutoffs were changed, while the result estimated with EMD only increases by 0.06 m/s. This suggests that the EMD can facilitate the removal of residual motion and providing of robust measurements.

PROSE was shown to be effective in both phantom and *in vivo* liver studies. The shear wave speed reported in the homogenous phantom agreed with that obtained with the Logiq E9, and the shear wave speed image from the phantom was smooth with a relatively small standard deviation. For all five volunteers, PROSE was in good agreement with the ARF measurements obtained with the Logiq E9. In some cases, a smaller ROI was selected corresponding to regions with good shear wave propagation; however, the area within the ROI was many times larger than that of conventional ARF methods, allowing PROSE to obtain measurements over larger areas which may provide a more comprehensive evaluation of the liver.

Theoretically PROSE is able to obtain shear wave speed estimates from a single frame of shear wave motion. In the case that the shear wave signal-to-noise ratio is poor, it is possible to leverage the periodicity of the shear waves to perform frame averaging to improve signal-to-noise ratio. An additional consideration is that this method allows for the compression artifact to be removed from all temporal frames, which would allow the use of additional shear wave estimation methods such as time-of-flight or phase gradient for reconstruction.

In phantom experiments, a 100 Hz vibration frequency was able to provide shear waves that reached the bottom of the phantom. For the *in vivo* study, a lower vibration frequency of 30 Hz was used to produce shear waves able to penetrate through the entire liver. One limitation of the selection of a low vibration frequency is that the resulting wave field has increased wavelengths. The LFE is unable to instantaneously transition across boundaries with different stiffness, and instead gradually transitions between the two regions. The width of the transition region has been estimated to be approximately a half wavelength [35], and thus the low vibration frequency used may not be able to resolve small areas of different stiffness. However, liver fibrosis is widely considered as a diffuse disease for elastography

Author Manuscript Author Manuscript Author Manuscript Author Manuscript

measurements [34], making it a good application for this method. A second limitation is that the imaging plane is 2D and thus is susceptible to out-of-plane waves, which could lead to elevated shear wave speed estimates [8]. While the axial vibration of PROSE was designed to minimize these effects, in order to image through the intercostal spaces the probe was in contact with the ribs, which may act as additional vibration sources and contribute to the complicated wave field. It is expected that this issue can be resolved by moving to a 3D acquisition [36].

PROSE was successful in demonstrating its ability to generate and detect shear waves in the liver from five healthy volunteers. There was good agreement between the shear wave speeds reported with PROSE and with the Logiq E9. This suggests that PROSE has promise as an effective shear wave elastography method. Since PROSE utilizes mechanical vibrations to generate shear waves, it is not limited by the mechanical or thermal index like ARF-based methods. In addition, the method has good penetration, making it attractive for patients with a high body mass index. Future studies will be conducted to explore the effects of the vibration frequency on shear wave signal quality and penetration, optimize the vibration system to further improve the efficacy of PROSE for liver fibrosis staging, and examine the stiffness at various points on the respiration cycle.

V. Conclusion

The complicated wave fields detected in PROSE from a continuously moving probe can be decoupled to isolate shear waves using the EMD method. This allowed for stable reconstructions that were not affected by selection of bandpass filtering cutoffs. A real-time shear wave display was used to improve probe placement for *in vivo* liver imaging. Shear wave speed measurements of a phantom and in the livers of five volunteers showed good agreement with ARF based shear wave elastography, but provided measurements for much larger regions. These results demonstrate the feasibility of PROSE as a 2D ultrasound elastography technology with the advantages of deep penetration, large field-of-view, and real time imaging.

Acknowledgments

This work was supported by the National Institutes of Health (NIH) under Grant R01DK106957 and Grant R21AR069850. The content is solely the responsibility of the authors and does not necessarily represent the official views of the NIH.

References

1. Nightingale K, McAleavey S, Trahey G. Shear-wave generation using acoustic radiation force: In vivo and ex vivo results. Ultrasound Med Biol. Dec.2003 29:1715–1723. [PubMed: 14698339]
2. Sandrin L, Fourquet B, Hasquenoph JM, Yon S, Fournier C, Mal F, Christidis C, Ziol M, Poulet B, Kazemi F, Beaugrand M, Palau R. Transient elastography: A new noninvasive method for assessment of hepatic fibrosis. Ultrasound Med Biol. Dec.2003 29:1705–1713. [PubMed: 14698338]
3. Bercoff J, Tanter M, Fink M. Supersonic shear imaging: A new technique for soft tissue elasticity mapping. IEEE Trans Ultrason, Ferroelectr, Freq Control. Apr.2004 51:396–409. [PubMed: 15139541]

Author Manuscript Author Manuscript Author Manuscript Author Manuscript

4. McAleavey SA, Menon M, Orszulak J. Shear-modulus estimation by application of spatially-modulated impulsive acoustic radiation force. Ultrason Imaging. Apr.2007 29:87–104. [PubMed: 17679324]

5. Yin M, Talwalkar JA, Glaser KJ, Manduca A, Grimm RC, Rossman PJ, Fidler JL, Ehman RL. Assessment of hepatic fibrosis with magnetic resonance elastography. Clinical Gastroenterology and Hepatology. Oct.2007 5:1207–1213. [PubMed: 17916548]

6. Chen S, Urban MW, Pislaru C, Kinnick R, Zheng Y, Yao AP, Greenleaf JF. Shearwave Dispersion Ultrasound Vibrometry (SDUV) for Measuring Tissue Elasticity and Viscosity. IEEE Trans Ultrason, Ferroelectr, Freq Control. Jan.2009 56:55–62. [PubMed: 19213632]

7. Song P, Zhao H, Manduca A, Urban MW, Greenleaf JF, Chen S. Comb-Push Ultrasound Shear Elastography (CUSE): A Novel Method for Two-Dimensional Shear Elasticity Imaging of Soft Tissues. IEEE Trans Med Imag. Sep.2012 31:1821–1832.

8. Zhao H, Song P, Meixner DD, Kinnick RR, Callstrom MR, Sanchez W, Urban MW, Manduca A, Greenleaf JF, Chen S. External Vibration Multi-Directional Ultrasound Shearwave Elastography (EVMUSE): Application in Liver Fibrosis Staging. IEEE Trans Med Imag. Nov.2014 33:2140–2148.

9. Manduca A, Oliphant TE, Dresner MA, Mahowald JL, Kruse SA, Amromin E, Felmlee JP, Greenleaf JF, Ehman RL. Magnetic resonance elastography: non-invasive mapping of tissue elasticity. Medical Image Anal. Dec.2001 5:237–54.

10. Knutsson H, Westin CF, Granlund GH. Local multiscale frequency and bandwidth estimation. Proc IEEE Int Conf Image Processing. 1994

11. Oliphant TE, Manduca A, Ehman RL, Greenleaf JF. Complex-valued stiffness reconstruction for magnetic resonance elastography by algebraic inversion of the differential equation. Mag Reson Med. Feb.2001 45:299–310.

12. Catheline S, Benech N. Longitudinal shear wave and transverse dilatational wave in solids. The J Acoust Soc Amer. Feb.2015 137:EL200–5. [PubMed: 25698051]

13. Sandrin L, Tanter M, Gennisson JL, Catheline S, Fink M. Shear elasticity probe for soft tissues with 1-D transient elastography. IEEE Trans Ultrason, Ferroelectr, Freq Control. Apr.2002 49:436–46. [PubMed: 11989699]

14. Sandrin L, Fourquet B, Hasquenoph JM, Yon S, Fournier C, Mal F, Christidis C, Ziol M, Poulet B, Kazemi F, Beaugrand M, Palau R. Transient elastography: a new noninvasive method for assessment of hepatic fibrosis. Ultrasound Med Biol. Dec.2003 29:1705–13. [PubMed: 14698338]

15. Song P, Macdonald M, Behler R, Lanning J, Wang M, Urban M, Manduca A, Zhao H, Callstrom M, Alizad A, Greenleaf J, Chen S. Two-dimensional shear-wave elastography on conventional ultrasound scanners with time-aligned sequential tracking (TAST) and comb-push ultrasound shear elastography (CUSE). IEEE Trans Ultrason, Ferroelectr, Freq Control. Feb.2015 62:290–302. [PubMed: 25643079]

16. Sarvazyan AP, Rudenko OV, Swanson SD, Fowlkes JB, Emelianov SY. Shear wave elasticity imaging: a new ultrasonic technology of medical diagnostics. Ultrasound Med Biol. Nov.1998 24:1419–35. [PubMed: 10385964]

17. Yamakoshi Y, Sato J, Sato T. Ultrasonic imaging of internal vibration of soft tissue under forced vibration. IEEE Trans Ultrason, Ferroelectr, Freq Control. 1990; 37:45–53. [PubMed: 18285015]

18. Bamber J, Cosgrove D, Dietrich CF, Fromageau J, Bojunga J, Calliada F, Cantisani V, Correas JM, D'Onofrio M, Drakonaki EE, Fink M, Friedrich-Rust M, Gilja OH, Havre RF, Jenssen C, Klauser AS, Ohlinger R, Saftoiu A, Schaefer F, Sporea I, Piscaglia F. EFSUMB guidelines and recommendations on the clinical use of ultrasound elastography. Part 1: Basic principles and technology. Ultraschall in Der Medizin. Apr.2013 34:169–84. [PubMed: 23558397]

19. Mellema DC, Song P, Kinnick RR, Urban MW, Greenleaf JF, Manduca A, Chen S. Probe Oscillation Shear Elastography (PROSE): A High Frame-Rate Method for Two-Dimensional Ultrasound Shear Wave Elastography. IEEE Trans Med Imag. Sep.2016 35:2098–106.

20. Catheline S, Wu F, Fink M. A solution to diffraction biases in sonoelasticity: the acoustic impulse technique. J Acoust Soc Amer. May.1999 105:2941–50. [PubMed: 10335643]

21. Huang NE, Shen Z, Long SR, Wu MLC, Shih HH, Zheng QN, Yen NC, Tung CC, Liu HH. The empirical mode decomposition and the Hilbert spectrum for nonlinear and non-stationary time

Author Manuscript Author Manuscript Author Manuscript Author Manuscript

series analysis," Proc. of the Royal Soc. of London: Math. Physical and Eng Sci. Mar 8.1998 454:903–995.

22. Montaldo G, Tanter M, Bercoff J, Benech N, Fink M. Coherent Plane-Wave Compounding for Very High Frame Rate Ultrasonography and Transient Elastography. IEEE Trans Ultrason, Ferroelectr, Freq Control. Mar.2009 56:489–506. [PubMed: 19411209]
23. Kasai C, Namekawa K, Koyano A, Omoto R. Real-time two-dimensional blood flow imaging using an autocorrelation technique. IEEE Trans Sonics Ultrason. 1985
24. Salisbury JI, Wimbush M. Using modern time series analysis techniques to predict ENSO events from the SOI time series. Nonlinear Processes in Geophysics. May-Jul;2002 9:341–345.
25. Wang XJ. Neurophysiological and Computational Principles of Cortical Rhythms in Cognition. Physiological Rev. Jul.2010 90:1195–1268.
26. Peng ZK, Tse PW, Chu FL. A comparison study of improved Hilbert-Huang transform and wavelet transform: Application to fault diagnosis for rolling bearing. Mech Syst and Signal Process. Sep. 2005 19:974–988.
27. Huang NE, Wu ML, Qu WD, Long SR, Shen SSP. Applications of Hilbert-Huang transform to non-stationary financial time series analysis. Appl Stochastic Models in Bus and Industry. Jul-Sep; 2003 19:245–268.
28. Linderhed A. Image compression based on empirical mode decomposition. Proc of SSAB Symp Image Anal. 2004:110–113.
29. Rilling G, Flandrin P, Goncalves P, Lilly JM. Bivariate empirical mode decomposition. IEEE Signal Process Lett. Dec.2007 14:936–939.
30. Looney D, Mandic DP. Multiscale Image Fusion Using Complex Extensions of EMD. IEEE Trans Signal Process. Apr.2009 57:1626–1630.
31. Bamberger RH, Smith MJT. A filter bank for the directional decomposition of images: Theory and design. IEEE Trans Signal Process. Apr.1992 40:11.
32. Lu YM, Do MN. Multidimensional directional filter banks and surfacelets. IEEE Trans Image Process. Apr.2007 16:918–31. [PubMed: 17405426]
33. Zhao H, Song P, Meixner DD, Kinnick RR, Callstrom MR, Sanchez W, Urban MW, Manduca A, Greenleaf JF, Chen S. External vibration multi-directional ultrasound shearwave elastography (EVMUSE): application in liver fibrosis staging. IEEE Trans Med Imag. Nov.2014 33:2140–8.
34. Barr RG, Ferraioli G, Palmeri ML, Goodman ZD, Garcia-Tsao G, Rubin J, Garra B, Myers RP, Wilson SR, Rubens D, Levine D. Elastography Assessment of Liver Fibrosis: Society of Radiologists in Ultrasound Consensus Conference Statement. Radiology. Sep.2015 276:845–61. [PubMed: 26079489]
35. Manduca A, Muthupillai R, Rossman PJ, Greenlead JF, Ehman RL. Image processing for magnetic resonance elastography". Proc SPIE. 1996; 2710:616–623.
36. Wang M, Byram B, Palmeri M, Rouze N, Nightingale K. Imaging transverse isotropic properties of muscle by monitoring acoustic radiation force induced shear waves using a 2-D matrix ultrasound array. IEEE Trans Med Imag. Sep.2013 32:1671–84.

Author Manuscript Author Manuscript Author Manuscript Author Manuscript

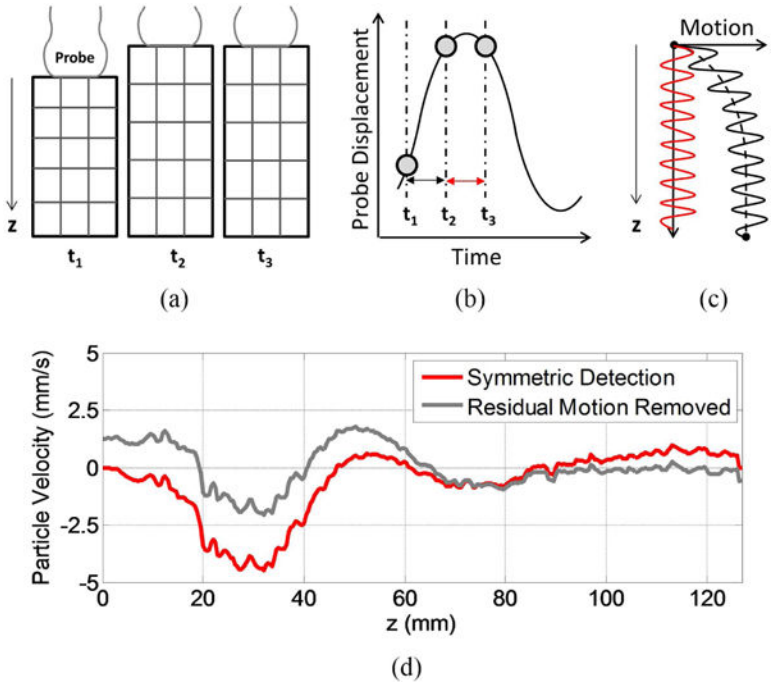

Fig. 1.

a) A continuously moving probe causes different deformations in the interrogated material at each time point. b) Pulse-echo ultrasound detects relative motion between two pulse-echo events. If detections are made when the probe is at separate physical locations (t_1-t_2), a resulting strain-like probe motion artifact is observed (c, black line). Theoretically if detections are made when the probe has returned to the same location (b, t_2-t_3), it is possible to suppress the artifact (c, red line). d) However, line-profiles from *in vivo* liver images show that this symmetric detection scheme does not fully decouple the shear waves (red line), requiring more advanced estimation methods to suppress residual motion (gray line).

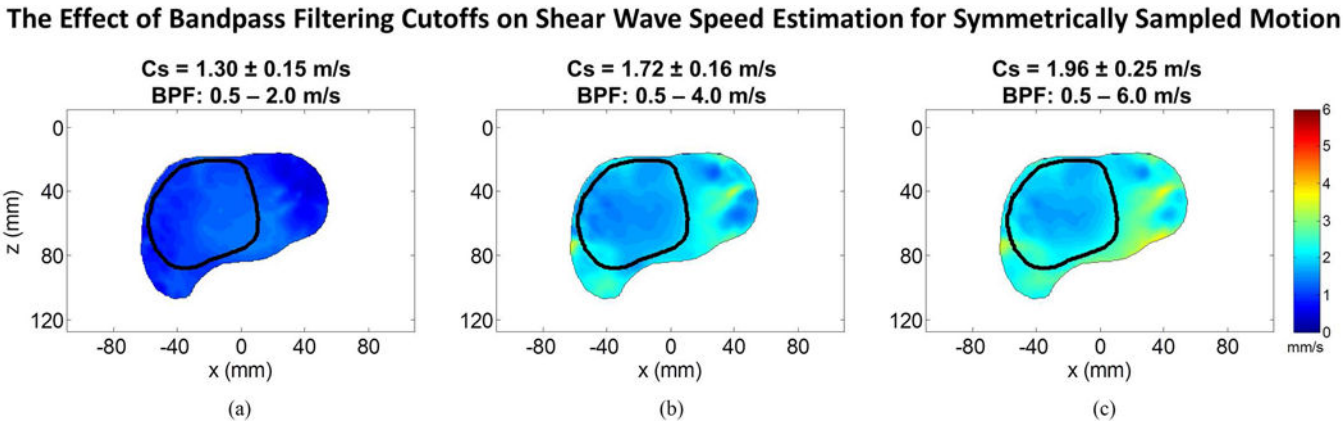

Fig. 2.

A test of bandpass frequency selection on shear wave speed reconstruction in liver of a healthy volunteer. A bandpass filter was applied to remove wavelengths corresponding to shear waves speeds outside a predetermined physiological range. The region-of-interest (ROI) was manually drawn to isolate areas with propagating shear waves. (a-c) Show the reconstructions using the symmetrical frame as the higher speeds (longer wavelengths) are added to the passband, resulting in the increased shear wave speed within the ROI.

Author Manuscript Author Manuscript Author Manuscript Author Manuscript

Author Manuscript Author Manuscript Author Manuscript Author Manuscript

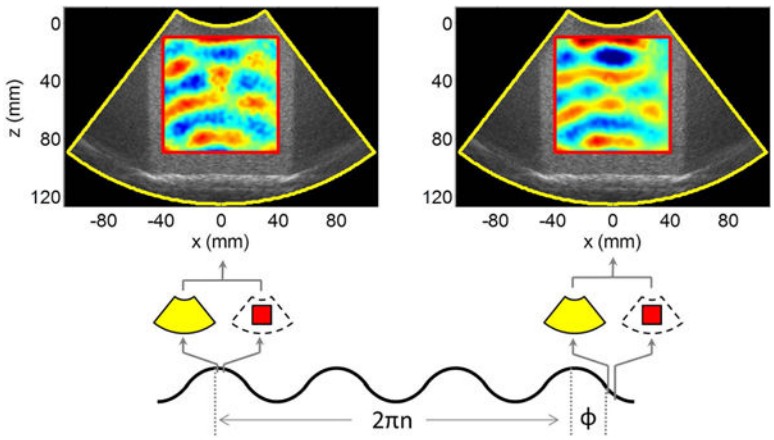

Fig. 3.

A timing diagram for the real-time visualization. This consists of two detections separated by 1 ms. The first detection acquires the full FOV and is used for B-mode guidance (yellow sector). The second is a square FOV (red box) that is used to compute shear wave motion. The time required to process and display the image is longer than a period; however, the periodic motion allows an integer number of cycles to be skipped before repeating the detection pairs to effectively sample every φ radians.

Author Manuscript Author Manuscript Author Manuscript Author Manuscript

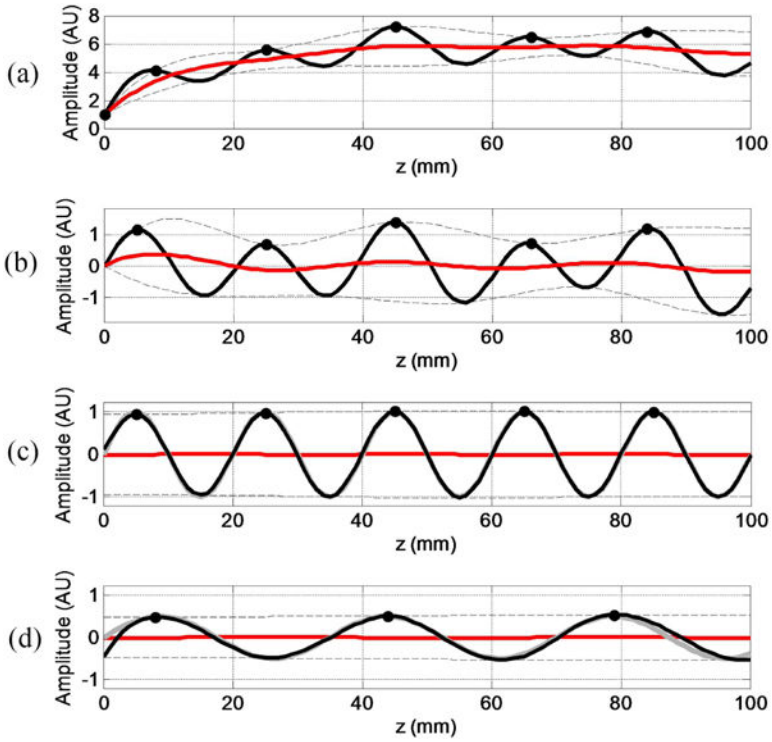

Fig. 4.

a) The solid black line represents an input function generated from a simulated compression and the summation of two sinusoidal shear waves. The top envelope (dashed) was obtained by fitting a spline through the local maxima (black dots). The midpoint of the top and bottom envelope is shown in red. b) After subtracting the midpoints from the input signal in (a) an estimate of the wave without the compression is shown as the black line. Since the midpoint is not sufficiently close to zero at all points, the sifting process is continued. c) The first IMF after sifting is complete (black) compared with the ground truth of the first sinusoid (grey). d) The second IMF (black) compared the ground truth of the second sinusoid (grey).

Author Manuscript Author Manuscript Author Manuscript Author Manuscript

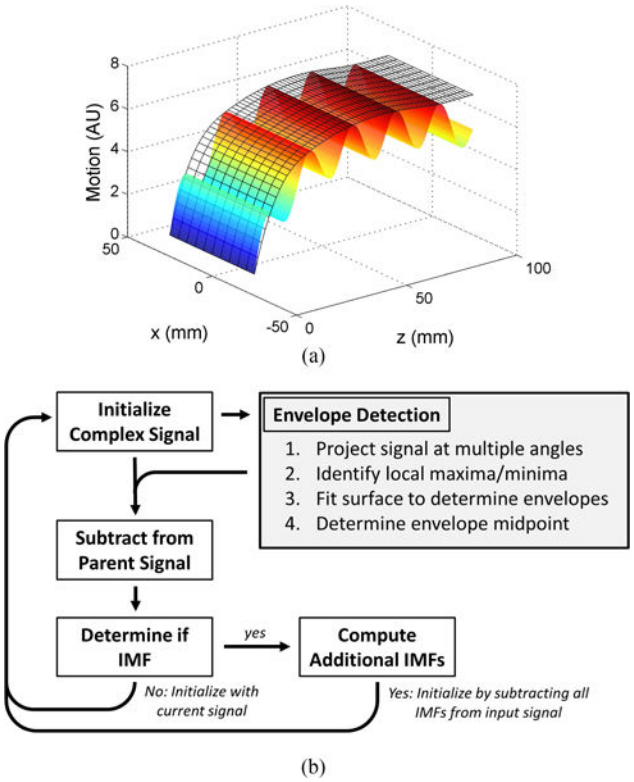

Fig. 5.

a) The 2D envelope obtained from a 2D simulated shear wave and compression artifact. b) A flowchart depicting the complex EMD process.

Author Manuscript Author Manuscript Author Manuscript Author Manuscript

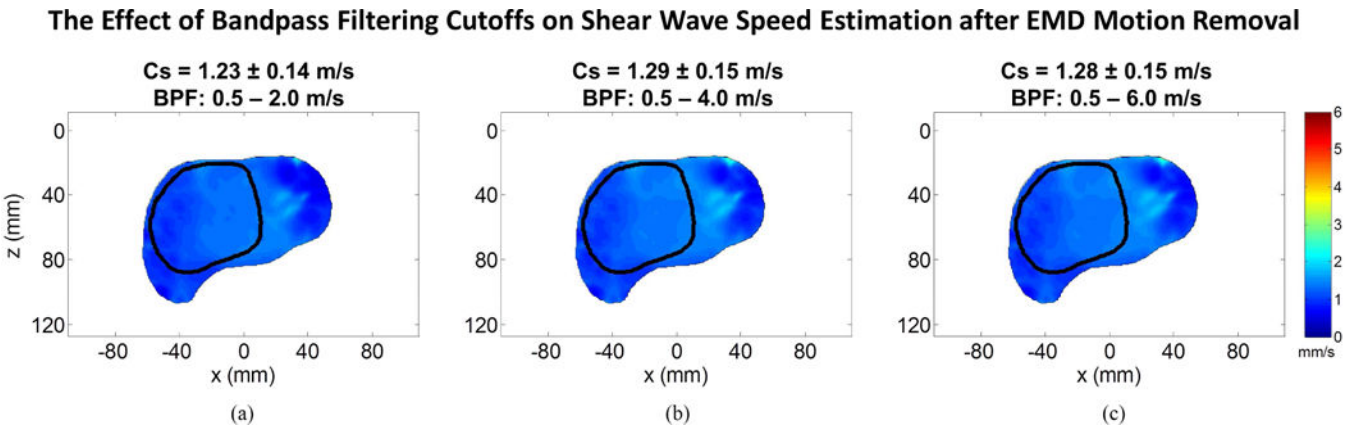

Fig. 6.

A test of bandpass frequency selection on shear wave speed reconstruction in liver of a healthy volunteer after utilizing the EMD to remove the residual motion. The region-of-interest (ROI) was manually drawn to isolate areas with propagating shear waves. (a-c) Show the reconstructions using the symmetrical frame as the higher speeds (longer wavelengths) are added to the passband, and demonstrates the ability of the EMD provide improved shear wave speed stability compared to the estimation without residual motion removal (Fig. 2).

Author Manuscript Author Manuscript Author Manuscript Author Manuscript

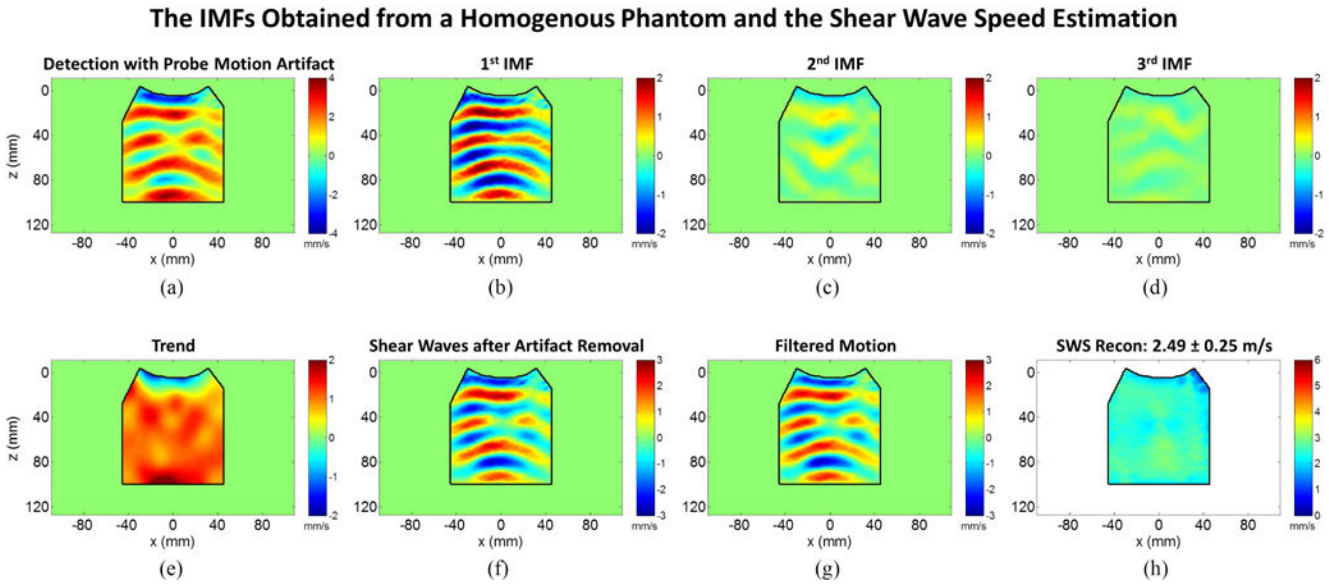

Fig. 7.

a) A representative frame of the detected motion from a tissue mimicking phantom with a 100 Hz vibration frequency. b-d) The first three IMFs that were decomposed from the signal. e) The residual signal (trend) which represents the probe motion artifacts containing no shear wave information. f) The shear waves after artifact removal. g) The bandpass filtered shear waves of (f). h) The LFE reconstruction of shear wave speed from (g) showed good agreement with the General Electric Logiq E9 (2.46 ± 0.06 m/s).

Author Manuscript Author Manuscript Author Manuscript Author Manuscript

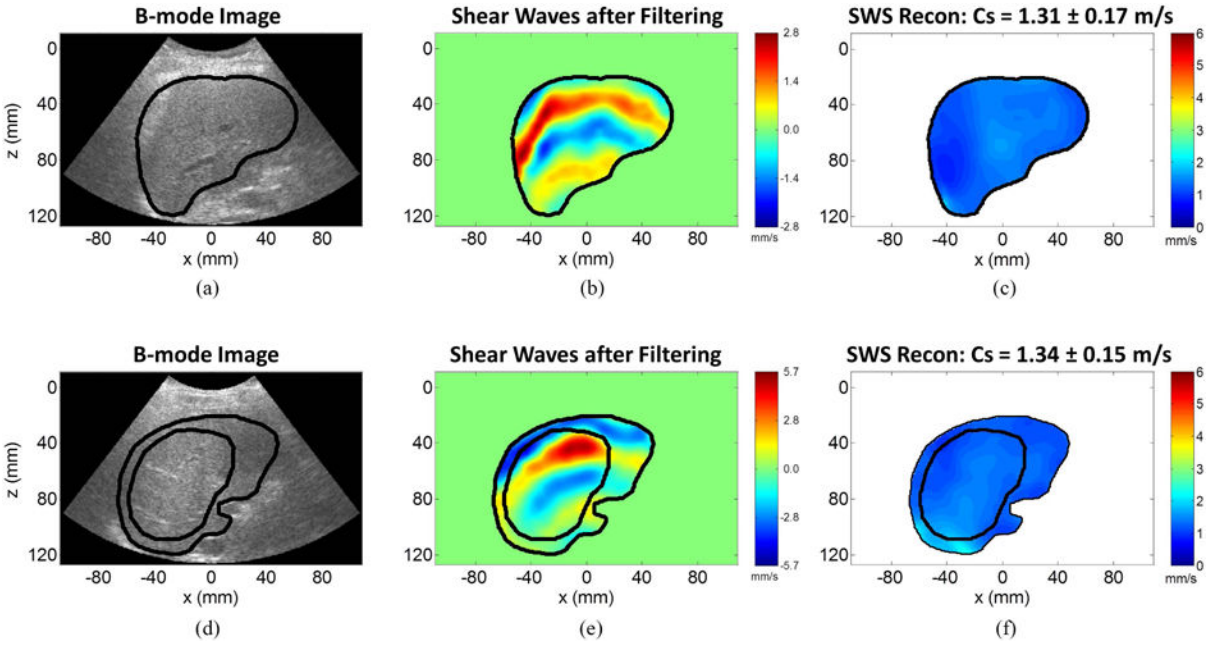

Fig 8.

a,d) B-mode images from two healthy volunteers obtained with a 30 Hz vibration frequency. The large ROI denotes the boundary of the liver while the small ROI denotes areas with clear shear wave signal. The large and small ROI for the top row are the same because there are good shear waves covering the entire liver. b,e) The resulting shear wave signal after EMD. c,f) The shear wave reconstruction was able to generate shear wave speed images with good agreement to the General Electric Logiq E9 (1.28 ± 0.06 and 1.43 ± 0.11 respectively).

Author Manuscript Author Manuscript Author Manuscript Author Manuscript

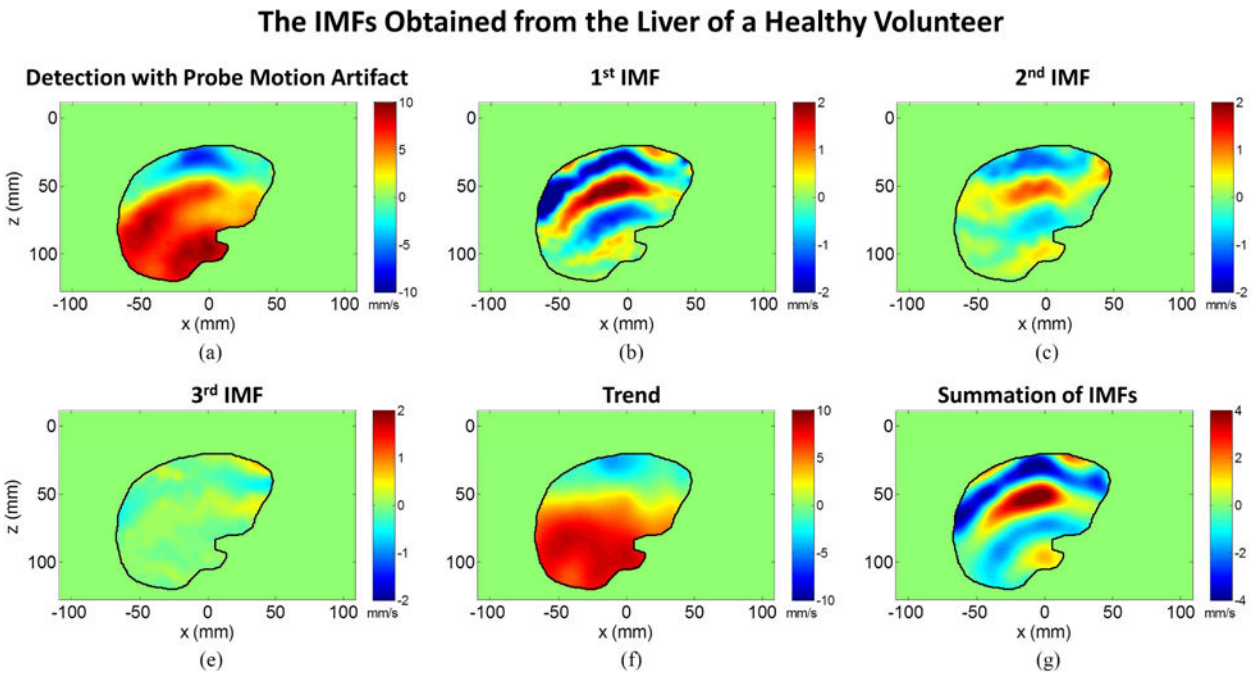

Fig. 9.

The decomposition of the motion from the healthy volunteer shown in second row of figure 8. a) A single frame of the detected motion containing the observable probe motion artifact and shear waves. b-d) The first three IMFs that were decomposed from the signal. These IMFs contain shear wave information. e) The residual signal (trend) which represents the probe motion artifacts containing no shear wave information. f.) The shear wave motion after artifact removal and bandpass filtering.

Author Manuscript Author Manuscript Author Manuscript Author Manuscript

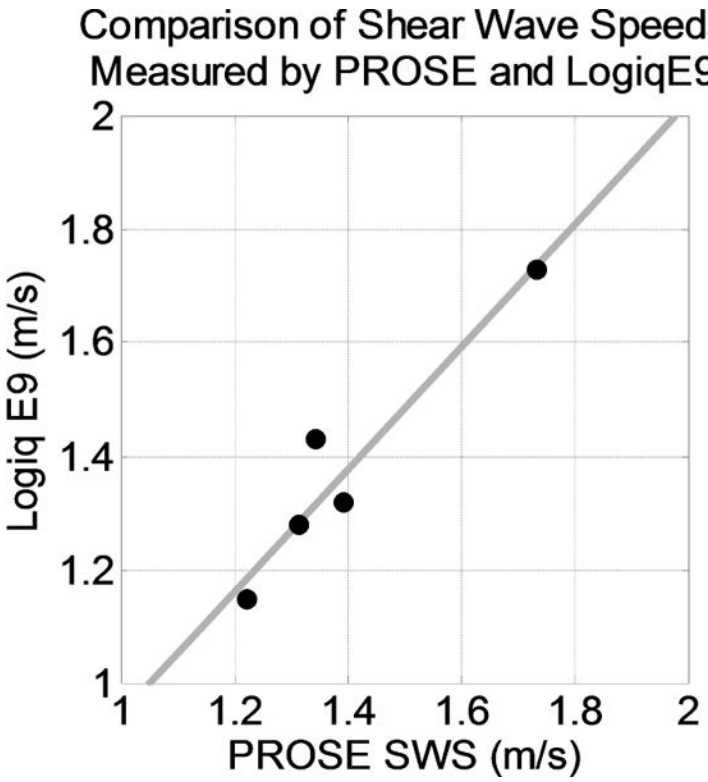

Fig. 10.

A comparison of the mean shear wave speeds measured with PROSE and the General Electric Logiq E9 in five healthy volunteers. The data were fit to a linear model resulting in a slope of 1.068. A Pearson's correlation coefficient of 0.955 (95% confidence 0.463 to 0.997) with a p-value of 0.0113 was achieved.

Author Manuscript Author Manuscript Author Manuscript Author Manuscript

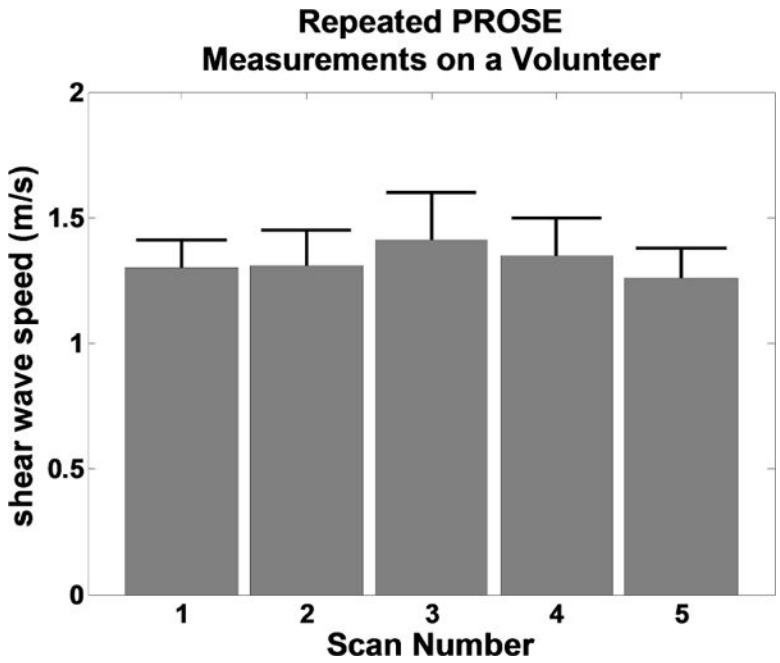

Fig. 11.

The mean shear wave speeds acquired from a healthy volunteer for five repeated trials, error bars denote standard deviation of the shear wave speeds within the ROI. The mean and standard deviation of the mean shear wave speeds reported for all five trials was 1.33 ± 0.06 m/s.

Author Manuscript

Author Manuscript

Author Manuscript

Author Manuscript

Table I

Shear Wave Speed of In Vivo Liver

A comparison of the shear wave speeds between PROSE and the GE Logiq E9. The shear wave speeds reported in PROSE were the mean and standard deviation of shear wave speeds within the ROI of a single acquisition, while the values for the Logiq E9 were the mean and standard deviation of the mean shear wave speeds from five repeated measurements (each measurement was the mean shear wave speed within the ROI of a single acquisition). The standard deviations are thus not comparable.

Volunteer	PROSE (m/s)	Logiq E9 (m/s)
1	1.34 ±0.15	1.43 ±0.11
2	1.73 ±0.24	1.73 ±0.17
3	1.31 ±0.17	1.28 ±0.06
4	1.25 ±0.10	1.15 ±0.02
5	1.39 ±0.12	1.32 ±0.02